EUROPEAN COMMISSION

Community Research

MATISSE

Materials' Innovations for Safe and Sustainable nuclear in Europe

Support to the development of joint research actions between national programmes on advanced nuclear materials

FP7-Fission-2013
Combination of Collaborative project (CP) and Coordination and Support Actions (CSA)

Grant agreement no: 604862
Start date: 01/11/2013 Duration: 48 Months

D.2.13

Advanced atomistic and object kinetic Monte Carlo models describing the decoration of loops by Cr, and the formation of Cr-Ni-Si-P clusters in Fe-alloys under irradiation

---

MatISSE – Contract Number: 604862

Document title	Advanced atomistic and object kinetic Monte Carlo models describing the decoration of loops by Cr, and the formation of Cr-Ni-Si-P clusters in Fe-alloys under irradiation
Author(s)	N. Castin, M. Chiapetto, G. Bonny, L. Malerba (SCK•CEN, Mol, Belgium) M. J. Caturla, J. P. Balbuena (UA, Alicante, Spain) C.C. Fu, R. Herschberg, T. Jourdan, E. Meslin, F. Soisson (SRMP, CEA Saclay) O. Tissot (SRMA, CEA Saclay)
Number of pages	22
Document type	Deliverable
Work Package	2
Document number	D2.13
Issued by	SCK•CEN
Date of completion	17/11/2017
Dissemination level	Confidential, only for consortium members (including the Commission Services)

Summary

In this work, we significantly improved kinetic Monte Carlo models aimed at describing the formation of Cr-Ni-Si-P clusters, responsible for hardening and embrittlement ferritic/martensitic alloys. Three different tasks were performed in the framework of the MATISSE project, as summarized in this document: (a) an atomistic model describes the formation of α' precipitates in FeCr alloys; including the radiation-increased concentration of point-defects, an atomistic kinetic Monte Carlo (AKMC) model is employed for accurately describing the so-induced acceleration of precipitation; (b) enhanced object kinetic Monte Carlo models describe the microscopic changes taking place under neutron irradiation. Direct prediction for the formation of dilute solute-rich clusters are performed, achieving good agreement with the APT experimental evidence. Our results are globally discussed, and some perspectives for future investigation are suggested.

Approval

Rev.	Date	First author	WP leader	Project Coordinator
0	October/2017	N. Castin, SCK•CEN 16.10.2017	L. Malerba, SCK•CEN 23.10.2017	P.F. Giroux, CEA 17/11/2017

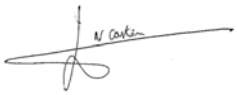
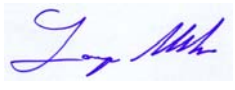


Distribution list

Name	Organisation	Comments
All beneficiaries	MatISSE	

Table of contents

1 Introduction

Ferritic/martensitic steels are structural materials for core components of GenIV sodium-fast reactor prototypes and remain primary candidate for commercial GenIV fast reactors, because they exhibit swelling resistance and good thermal conductivity. They are, however, penalized by other issues, that delay their design codification. The most serious issue is low-temperature (below 350-400°C) hardening and embrittlement, accompanied by severe plastic-flow localization. The origin of these must be found at the level of microstructural changes produced by irradiation in the material.

Recent investigations on model alloys for RAFM steels containing 2.5, 5, 9 and 12 %Cr (as well as a range of uncontrolled impurities) have revealed that three populations of defects contribute to low temperature radiation hardening, namely: (a) dislocation loops visible in TEM [1,2]; (b) α' precipitates detected by both atom probe tomography (APT) [3] and small angle neutron scattering (SANS) [4]; (c) supposedly most importantly of all, 3-4 nm diameter diffuse CrSiPNi solute clusters, invisible in TEM, but formed in similarly high density (~10^{23} m^{-3}) at all Cr contents, both under neutron and ion irradiation, as revealed by APT [3,5].

These dilute CrSiPNi clusters, formed under neutron irradiation at ~290°C, have been identified as the main contributors to the radiation-hardening measured in tensile tests [6, 7]. Their composition does not correspond to any known thermodynamic phase, and the contained impurities are present in the alloy in very low concentration, thereby suggesting an irradiation-induced origin [3,5,8,9]. Their actual structure remains elusive because they are difficult to see experimentally. No technique, even in combination with others, is able to tell anything fully conclusive about the possible association with radiation-defects of the solute clusters in the focus here. In some cases, these solute clusters have been found by APT to take a loop shape, or to have a roughly planar shape, with orientation consistent with the Burgers vectors of dislocation loops [3,8,9], suggesting heterogeneous precipitation of solutes on point-defect clusters as formation mechanism. Their actual structure, however, remains elusive and, in order to fully assess it, the support of appropriate atomistic models is essential, see e.g. [10], while microstructure evolution models are required to probe possible formation mechanisms, also in order to identify which solute atoms are most effective to produce this segregation and whether or not minor alloying elements may act as driving force to induce/enhance it.

The fact that these clusters contribute significantly to hardening clearly suggests a complex structure. If they were merely dilute and coherent solute clusters, dislocations would not be strongly pinned by them. In turn, dislocation loops below the resolution of the electron microscope should be easily absorbed by dislocations, providing negligible contribution to radiation-hardening [11]. However, the association of solutes and loops may be the explanation for their role on hardening [12], and, in connection with this, the role of minor alloying elements needs to be clarified. Here, too, the contribution of modelling to assess their strength as obstacles to dislocation motion, is key [12].

In the work reported here, we significantly improved kinetic Monte Carlo models aimed at describing the formation of the above-mentioned nano-features responsible for hardening and embrittlement of ferritic-martensitic alloys. Three different tasks were performed in the framework of the project. In section 2, the first one is reported: an atomistic kinetic Monte Carlo (AKMC) model has been developed to describe the formation of α' precipitates, including the radiation-increased concentration of point-defects and the so-induced acceleration of precipitation. Next, section 3 collects the contributions that concern the development of enhanced object kinetic Monte Carlo (OKMC) models, aimed at describing the microscopic changes taking place under neutron irradiation. Direct predictions of the formation of dilute solute-rich clusters are made, achieving good agreement with the APT experimental evidence. Section 4 summarizes and suggests perspectives for future investigation.

2 Radiation-enhanced precipitation of Cr in Fe

In this section, we report atomistic models to describe the precipitation of the Cr-rich α' phase in ferritic alloys. At temperatures below 300°C, alloys with more than ~9%Cr are supersaturated, but the α' precipitation is too slow to be observed during thermal ageing on accessible times, due to slow diffusion coefficients. Irradiation increases point defect concentrations and therefore accelerates the diffusion of substitutional elements, and the precipitation kinetics. Our objective was to model this behaviour, to quantify the acceleration and the ballistic mixing, which may have opposite effects, i.e. the formation and dissolution of α' precipitates, respectively. The effect of carbon atoms (and others interstitials impurities: O and N) which are present in ferritic steels and strongly interact with vacancies, has been also studied.

2.1 Methodology: AKMC simulations

These phenomena have been modelled by atomistic kinetic Monte Carlo (AKMC) simulations, previously used to study radiation induced segregation in Fe-Cr alloys [13]. The AKMC code is based on a diffusion model that takes into account the key mechanisms controlling the precipitation kinetics: the creation of point defects by elastic collisions, the diffusion of vacancies and self-interstitials atoms (with their dumbbell configurations), their elimination by mutual recombination or annihilation at sinks (dislocations, grain boundaries, point defects clusters, etc.). The AKMC parameters have been determined by DFT calculations of mixing and point defect properties. Cluster dynamics was used to estimate the evolution of the sink density and sink strengths under irradiation. For each irradiation conditions, the cluster dynamics parameters have been fitted on experimental observations of the densities point defect clusters [14,15].

2.2 Results and discussion

2.2.1 Kinetics of α' precipitation under electron, neutron and ion irradiation

The α' precipitation has been first model in binary Fe-Cr alloys under neutron irradiation at a low dose rates [14], and compared with 3D atom probe (3DAP) experiments by Bachhav et al. [16]. The simulations have shown that the precipitation kinetics strongly depends on the evolution of the sink density that controls the point defect concentrations under irradiation, and therefore the Fe and Cr diffusion coefficients. The evolution of the sink density was estimated by cluster dynamics, and its consequence on the point defect concentration was indirectly taken into account through a rescaling of the Monte Carlo time [14]. Neutron irradiation was found to accelerate the precipitation by several orders of magnitude, with no significant effect of ballistic mixing.

These first simulations indicated that it was important to explicitly take into account the evolution of the sink density in the AKMC simulations, especially for irradiations at higher dose rates when ballistic mixing becomes significant. Simulations with variable sink densities (again predicted cluster dynamics results) have been developed and applied to the modelling of α' precipitation under electron, neutron, and ion irradiations at various dose rates [15]. They show strong accelerations of the precipitation kinetics under electron, neutron and ion irradiations at low or moderate dose rates, without significant effect of the ballistic mixing. Only under ion irradiation at very high dose rates (typically 10^{-3} dpa.s^{-1}), the ballistic mixing is found to prevent the formation of α' precipitates and even to dissolve existing precipitates. This ballistic dissolution is due to the very high sink densities that can be reached under such irradiation conditions, which limits the point defect supersaturation.

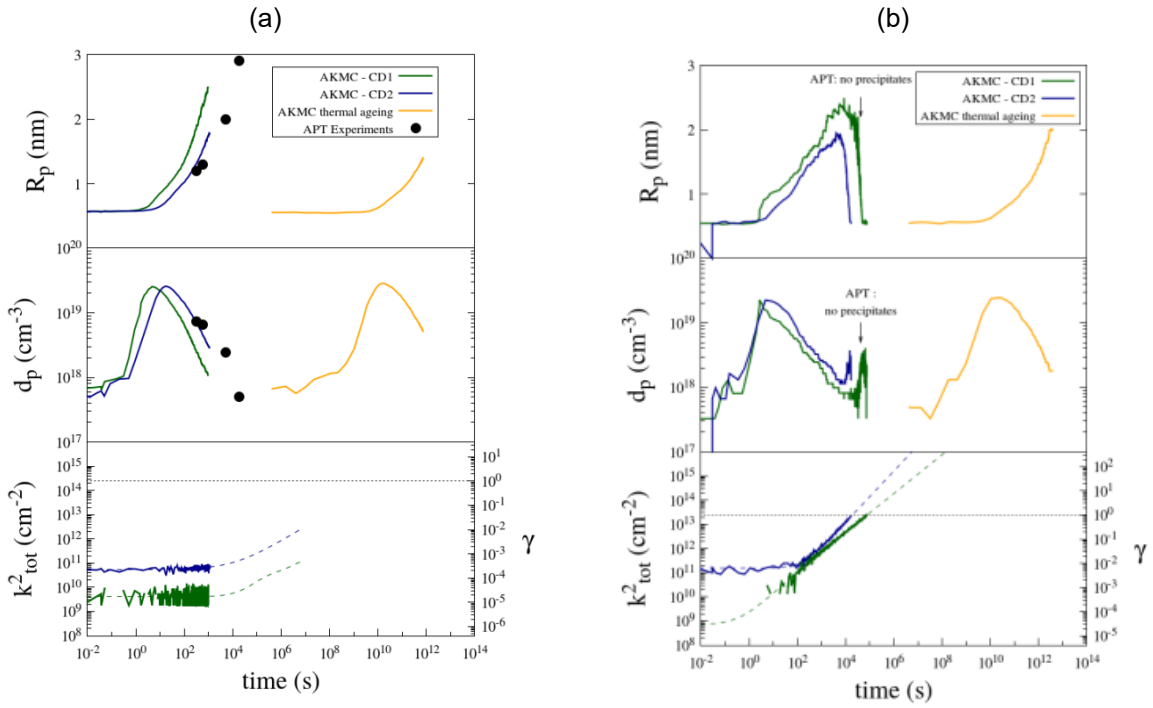

Fig. 2.1 – Evolution of the radius and density of α' precipitates, and of the total sink strength k^2_{tot} (proportional to the sink density) in Fe-15%Cr at 300°C, (a) under electron irradiations at 3.9 × 10^{-5} dpa.s^{-1}, (b) under ion irradiation at 2.8 × 10^{-3} dpa.s^{-1}. Comparison between 3DAP observations (black dots) and AKMC simulations (lines). The green lines correspond to a sink density without carbon atoms, the blue lines to a sink density with significant carbon contaminations.

2.2.2 Effect of carbon on the α' precipitation

Carbon atoms may affect the precipitation of Cr by reducing the mobility of point defects and, if the carbon concentration is sufficient, by precipitation of carbides. Only the first effect has been considered here. Preliminary AKMC simulations, using a simplified model of carbon diffusion in Fe-Cr alloys, suggested that for a given density of sinks, the strong binding between vacancy and carbon atoms may lead to a slowing down of the α' precipitation. The effect has been found to be significant when the carbon concentration is larger than the concentration of sinks, and when the annihilation of point defects by mutual recombination is not negligible. An important carbon concentration can also results in an increase in the sink density: this has been taken into account in the cluster dynamics and AKMC simulations with variable sink densities [15], this also contributes to the slowing down of the α' precipitation and favours ballistic dissolution.

2.2.3 Diffusion of carbon in Fe-Cr alloys – simulations of internal friction experiments

The previous results showed that it is important to develop a better description of carbon diffusion in Fe-Cr alloys. This has been done by introducing in AKMC simulations the diffusion of C in octahedral interstitial sites, with a dependence of the C migration barrier on the local Cr concentration fitted on DFT calculations. AKMC simulations have been compared to experimental tracer diffusion coefficients (in dilute Fe-Cr alloys [17]) and internal friction measurements (in dilute and concentrated alloys [18]): they show a continuous evolution of the Snoek peak and of the C migration energy which differs from the internal friction measurements, but are in agreement with tracer diffusion experiments. The origin of the discrepancy between the two experimental methods are under investigation. The diffusion model of C in Fe-Cr must now be implemented in AKMC simulations of α' precipitation under irradiation.

3 Radiation-induced formation of solute clusters

The Cr content in high-Cr F/M steels is known to have a strong effect on radiation defect stability and, in general, on the properties of the material. For this reason, Fe-Cr alloys are often employed as model materials in irradiation experiments and subsequent characterization. Minor alloying elements are also included, amongst which Ni, Si and P. In this section, we report the work performed for the development of physical models describing the microstructural changes in Fe-Cr-C-(NiSiP) model alloys under neutron irradiation.

As previously introduced, the primer objective in this work is to describe in detail the formation of CrNiSiP-rich clusters as observed in APT measurements. The proposed underlying mechanism is the transport, by single point defects, of the solute atoms (initially dissolved in the matrix) towards sinking sites in the bulk of the materials. Clearly, the microstructural changes taking place involve interplay of complex processes at the atomic level. To accomplish our modelling objective, we opted for an object kinetic Monte Carlo (OKMC) approach, because these models form a bridge between atomic-level events (such as in AKMC models) and continuum models such as cluster dynamics. In the former case, accurate transport of solutes may be implemented as a consequence of local point-defects migration events, while in the latter case larger-scale events governing the microstructure evolutions (e.g., irradiation events, loops/solute interaction, etc.) are dealt with.

In the following of this section, we describe how the work was divided in two separate, but convergent approaches, and performed in three distinct steps. We start, in section 3.1, by reporting the development of a base model, specifically dedicated to describe the evolution of the population of point defects. While no solutes are described in the studied materials, the lifetime of vacancy and SIA defects is followed through the whole irradiation period, thus making predictions for TEM-observable SIA loops and voids, and PAS-resolvable vacancy defects. Taking steps from previous works considering the pure Fe case [21], our OKMC model was extended to the FeCr system [22,23]. The validation is based on the assumption that the population of small SIA loops, as predicted by the model, is comparable in density with the APT-observed solute-rich clusters. This settles the base for a model assuming a radiation-induced mechanism for the formation for the solute clusters. Even though the Cr content obviously plays a central role in the parameterization, solute Cr atoms as such are not explicitly included in the model at this stage. Neither are, in the first version of the model, the other minor solutes, i.e., Ni, Si, and P. These are added later, in the model of section 3.2. Making simple assumptions, we show how the base model gives realistic predictions when the minor solutes are added in the matrix. Transport is parameterized assuming the infinite dilution limit, and also assuming simple schemes for the extra binding to SIA clusters by the decorating solutes. Last, in section 3.3, we report the development of a separate model specifically dealing with the Cr content, providing a description of the formation of α' precipitates within a cellular approach.

3.1 Basic object kinetic Monte Carlo model

The work reported in this section is thoroughly described in two scientific publications, authored by M. Chiapetto et al., in Ref. [22,23]. A summary is provided in the remaining of this section.

Object kinetic Monte Carlo (OKMC) models describe the microstructural applying suitable approximations. Atomic-scale events can be explicitly included if necessary, giving a detailed description of events such as the migration of point-defects, to a certain extent accounting for complex local chemical composition. In addition, the MC algorithm and the abstractions taken while describing bigger size defects (vacancy and SIA clusters) allows the simulation time and length scales to be extended significantly with respect to AKMC models. In Ref. [21], the specific case of the Fe-C system was addressed, which serves as a base for the present work.

In OKMC models irradiation events take place as stochastic inclusion of cascade debris, previously obtained in molecular dynamics simulations. These are the primer source of defects in the simulated bulk material, i.e., vacancy and SIA clusters of various sizes with explicit spatial coordinates. Migration and dissociation events are then defined for these defects, whose frequencies are parameterized as thermally-activated :

$$\Gamma^{(Mig)} = \Gamma_0 \exp\left(-E_m/kT\right) \quad (1)$$

Here, Γ_0 is the attempt frequency, E_m is the migration energy, k is Boltzmann's constant and T the absolute temperature. Both the attempt frequency and migration energy are required input parameters, and are a

function of defect type and size. In Ref. [21], for example, vacancy clusters were parameterized from a study performed using an advanced AKMC model [29], based on an interatomic potential. SIA clusters were parameterized from molecular dynamics studies, essentially assuming a constant migration energy (from very small clusters on) but an attempt frequency that gradually decreases with the cluster size. The last essential parameter in the model was to account for the presence of foreign interstitial C impurities. Taking simplifying assumptions, the latter were assumed to be found, at equilibrium conditions, into the form of stable C-Vac clusters. No explicit C impurities were thus included in the model. Instead, an equivalent population of C-based trapping elements was carefully parameterized, in terms of composition (single C atoms, C_2Vac clusters, etc.) and effective trapping energies with any point-defect clusters. The model was validated while comparing the predicted population of TEM-visible population of SIA loops and voids, and PAS-resolvable population of single vacancies and small vacancy clusters.

Cr was introduced in the model making three assumptions:

- Both experimental [30-33] and theoretical [34-38] studies suggest that one of the main effects of Cr on the nanostructural evolution under irradiation of Fe-Cr alloys is the reduction of the mobility of self-interstitial clusters (dislocation loops) versus temperature, especially for ½⟨111⟩ loops [24]. This mobility reduction is physically due to the attractive interaction between the Cr atoms dispersed in the solid solution and the crowdions that form the clusters. Consistently with these observations, we reduced the mobility of SIA clusters, by adapting the migration attempt frequencies as a function of the Cr content, as shown in Fig. 3.1. This change is applied on average, as a function of the global Cr content, not taking its precipitation to α' phases into account. It is thus a grey alloy approximation.
- For every Cr concentration, all clusters bigger than 4 SIAs are of ½⟨111⟩ type. Therefore, a relatively low migration energy (~0.1 eV) was assigned to them. Furthermore, we also assumed that these clusters are trapped by C atoms and C_2Vac complexes, with a trapping energy of 0.6 and 1.3 eV, respectively [39,40].
- Based on experimental assessment, we assumed that the C concentration in the matrix is 20 appm for the alloys containing 5, 9 and 12 %Cr and it is ~80 appm for the one containing 2.5 %Cr (in both cases significantly smaller than the C nominal content, which was in excess of 1000 appm), while in the alloy containing no Cr at all it was ~130 appm.

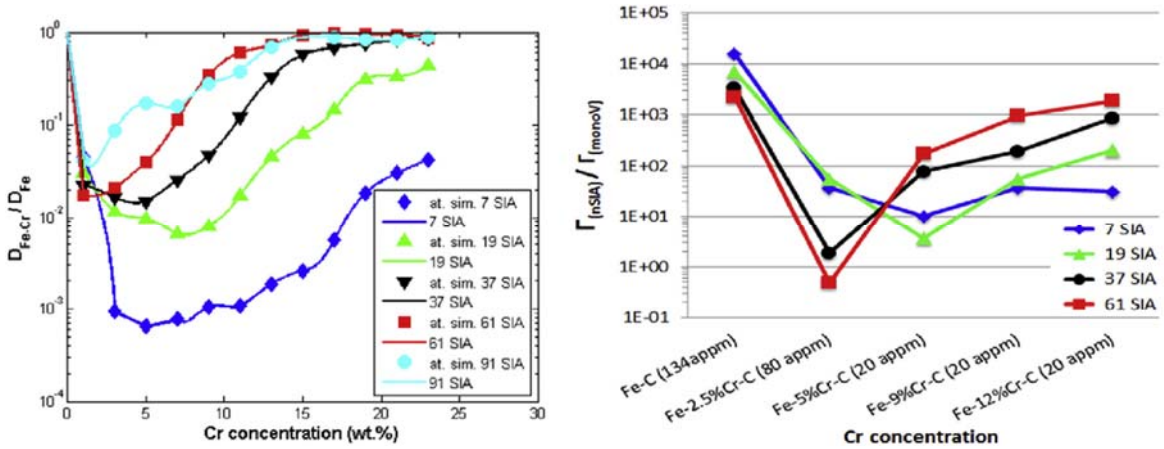

Fig. 3.1 – Non-monotonic trend of SIA cluster diffusivity reduction, normalized to the Fe-C alloy, as a function of Cr. On the left-hand side, atomic simulation ("at. sim.") data come from Ref. [26], while lines represent polynomial interpolations of the reference values. On the right-hand side, the ratios between the jump frequencies of SIA clusters normalized to that of the single vacancy, as a function of Cr content, are shown. The C concentration assumed to be left in the matrix, in our model, is also reported for all the alloys.

To validate the model, we conducted simulations of specific irradiation conditions for the Mire-Cr experiments performed in the BR2 reactor at SCK•CEN [25]. The materials were irradiated at ~290 °C (563 K) in a device that mimics the environmental conditions of a commercial pressurized water reactor. The dose rate was several orders of magnitudes higher, however: 10^{-7} dpa/s. The most essential results are summarized in Fig. 3.2 and Fig. 3.3 below.

In Fig. 3.2, the predicted density and size for TEM-visible SIA loops are compared with experimental measurements. We see that the model underestimates both, but nonetheless follows the right trend with increasing Cr content.

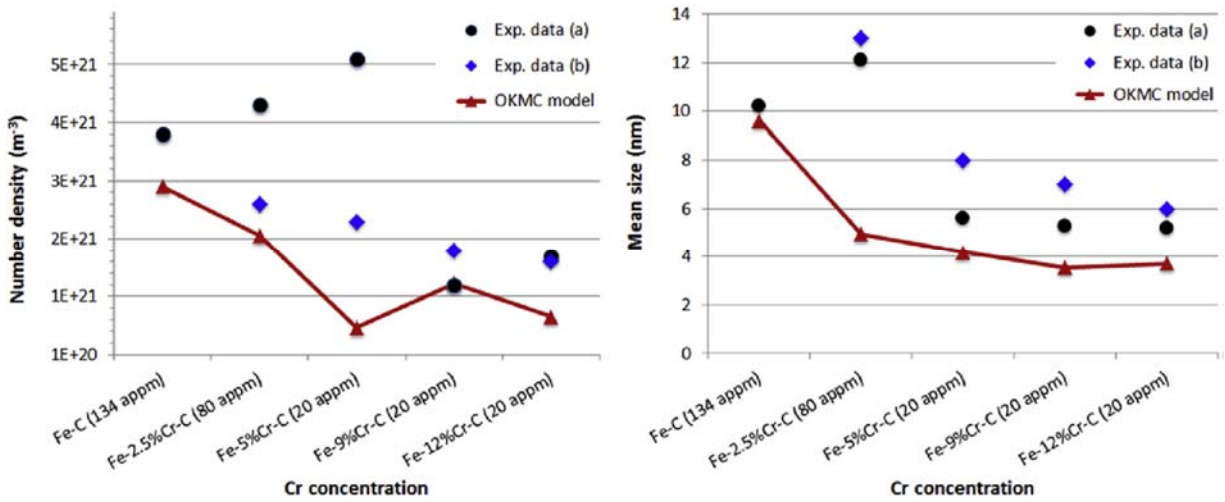

Fig. 3.2 – Number density (left) and mean size (right) versus Cr content of TEM-visible SIA clusters at 0.6 dpa (the OKMC model result for 2.5 %Cr is given for ~0.3 dpa). Both experimental and simulation results are given for 0.2 dpa. The assumed C concentration in the matrix for all model alloys is also reported. The experimental data (a) from Ref. [24] and (b) from Ref. [25] are also shown. Loops are considered visible in TEM if their radius is larger than ~1.3 nm (90 SIA) [21].

In Fig. 3.3, the predicted density and size for TEM-invisible SIA loops are shown. As already discussed above, the basic assumption made is to associate these with sinking sites for single point defects diffusing in the matrix. Assuming these point defects carry solute atoms (see section 3.2), we thus reasonably postulate that the small SIA loops are the nucleation sites for the formation of solute-rich clusters. The density of loops is thus directly compared with the density of solute-rich clusters as observed by APT. We see that the loops density in our model is lower, by up to no more than half an order of magnitude at the highest Cr concentration (but much higher than in pure Fe, due to the reduced mobility of SIA clusters). This discrepancy is acceptable. Considering that solute clusters are nucleated on SIA loops, the same loops are likely to either detach from the solutes (thermally-activated migration passing the extra barrier of the binding energy between the solutes and the loop), or to be eroded and finally annihilated by vacancies. It thus seems reasonable to assume that the density of loops is lower than the density of solute clusters, by less than an order of magnitude.

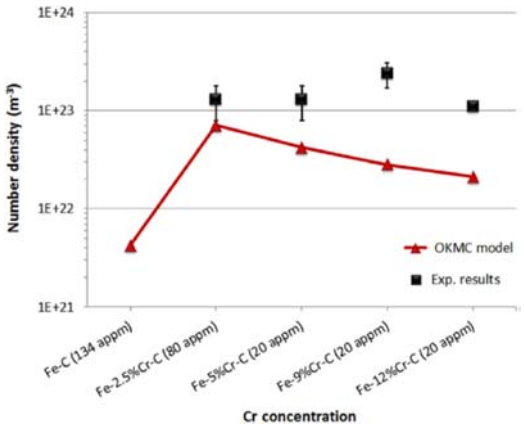

Fig. 3.3 – Number densities at 0.6 dpa of interstitial loops below TEM resolution, identified as NiSiPCr-enriched clusters, for different Cr content (the assumed C concentration in the matrix for all model alloys is also indicated). The OKMC results for Fe-C are at 0.2 dpa (see text). Squares are experimental data from APT [3]. SIA clusters between size 15 and 90 have been counted as solute clusters.

In conclusion, our results in this section provide evidence that tend to demonstrate our hypothetical scenario for the formation of solute-rich clusters. The matter cannot be investigated in more details, however, because the grey alloy model cannot describe solute redistribution. For this reason, the model needs to be upgraded, as described in section 3.2.

3.2 Inclusion of minor solutes elements

In this section, we describe how our microstructural model reported in section 3.1 was upgraded, including explicit treatment of minor solute elements (Ni, Si and P). These results are not yet published in the scientific literature, but a paper is in preparation.

Being a concentrated solute and thus requiring more profound changes in the model, Cr atoms as such are not included in the model at this stage. Consequently, the parameters describing the mobility and stability of point defects clusters remain identical as in the grey alloy approximation reported in section 3.1. Nevertheless, minor solute elements (Ni, Si and P) are included in the matrix, originally in random solution. They are assumed to be transported by single vacancies and single SIAs. Defining a capture radius (a_0), pairs may be formed. The mobility and stability of the pair is parameterized from DFT data obtained in Ref. [41, 42]. Assuming an infinite dilute limit, all possible vacancy or SIA migration energies were calculated, as a function of the presence of a solute nearby. The exact transport coefficients are thus deducible, making no further approximation.

Important information learned from Ref. [41, 42] is that all three minor solutes are transported by single vacancies in the temperature range of interest. Single SIA also transport P atoms in the same range of temperature, but not Si nor Ni. The following four new defects are thus added in the OKMC model: Vac-Ni pair, Vac-Si pair, Vac-P pair, and SIA-P pair. Once created, two events are defined for them: (a) the migration towards a 1nn position, thus provoking a transport of the carried solute; (b) separation, meaning that the point defect migrates towards a remote position, leaving the solute behind. It is important to note that, while other defects may temporarily carry solutes, they are not allowed to transport them. Indeed, solutes decorate point defects clusters, specifically small SIA loops immobilized by C traps, because incoming single vacancies or single SIA's carry them. If a migration event is chosen for the decorated loop, however, it is assumed to unbind from its solutes, leaving them behind at its initial position. This binding energy is a parameter that must be provided, as a function of the point defect cluster composition, and the content of solutes.

On the one hand, for simplicity, and in the absence of adequate energy data available (e.g. calculated with DFT or an adequate interatomic potential), the mobility of vacancy clusters are here assumed to be unaffected by decorating solutes. The migration energy for a vacancy clusters is thus unchanged taken from the pure Fe model, assuming that the binding energy with decorating solutes, if any, is negligible.

On the other hand, the mobility of SIA loops are assumed to be significantly affected by the decorating solutes. In this respect, DFT calculations were performed (C. Domain, EdF, France) for investigating the binding energies between loops and single solutes, as illustrated in Fig. 3.4. In the absence of more detailed data, we assumed that the binding energy between a loop and its decorating solutes reduces to the interaction with a single solute atom. In practice, the maximal value as reported in Fig. 3.4 was taken as effective binding energy. Concretely, if the cloud of decorating solutes includes at least one P atom, the value 1.1 eV is taken, because it is the solute exhibiting maximal binding at a particular position. If no P is there, but at least one Si atom, the binding energy is taken to be 0.45 eV. Finally, if only Ni atoms decorate the loop, the binding energy is taken to be 0.2 eV.

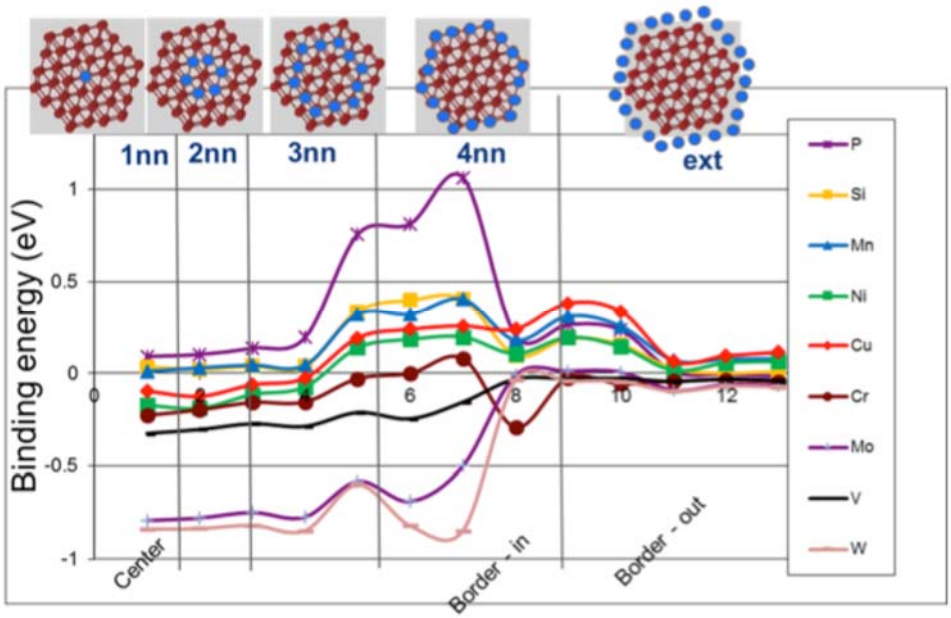

Fig. 3.4 – DFT-calculated binding energy between SIA loops and a single decorating solute element, as a function of its position along the loop. Results obtained by C. Domain et al. in the framework of MATISSE (deliverable D2.21.), unpublished.

Simulations were conducted in the same conditions as reported in section 3.1. The exact solute compositions are Fe–2.5%Cr–0.1%Si–0.019%P, Fe–9%Cr–0.057%Ni–0.065%Si–0.013%P, and Fe–12%Cr–0.07%Ni–0.18%Si–0.025%P.

Unsurprisingly, clouds of solute atoms are found to form at various locations in the simulation box. Direct comparison with the experimental measurements performed by APT requires two intermediate processing steps, as illustrated in Fig. 3.5.

- **Step 1: Atomic reconstruction.** Every defect containing solutes must be given a spatial substance, virtually introducing the solutes atoms in the matrix in a way as we assume they would be found in the real material. In the absence of more detailed information, we temporarily assumed that the solutes are configured in a compact way, being arranged as a sphere centred at the position of the defect. This point is discussed in more detail below.

- **Step 2: Mimic the APT.** Only about half of the atoms are detected by the atom probe and the spatial coordinates of the other atoms may be more or less distorted because of trajectory aberrations. These effects are taken into account while analysing the results of our OKMC model, in order to realistically reproduce the non-perfect efficiency of detection of solute clusters by APT. Inspired by collaborative discussions with colleagues [43,44], we established the following algorithm. (a) In order to account for the APT detection accuracy, 60% of the atoms in the simulation cell are chosen at random and discarded. (b) Since distortions in the atomic coordinates are inherently induced by the measurement, especially in the plane perpendicular to the sample main axis (very thin needle), the remaining atoms in the simulation cell are randomly displaced along that plane. The displacement magnitude follows a Gaussian distribution with a full width at half maximum (FWHM) as large as 0.75 nm, while a smaller value (0.1 nm) is applied in the direction of the sample axis. (c) Clusters are identified by searching for groups of neighbouring atoms, with a cutoff distance of $1.75a_0$ = 4.954 Å. The cluster radii are calculated with the Guinier formula. This procedure mimics the dissolution of small clusters of solute atoms at the beginning of the APT measurement, as well as the average increase of cluster size due to the APT-induced local displacements.

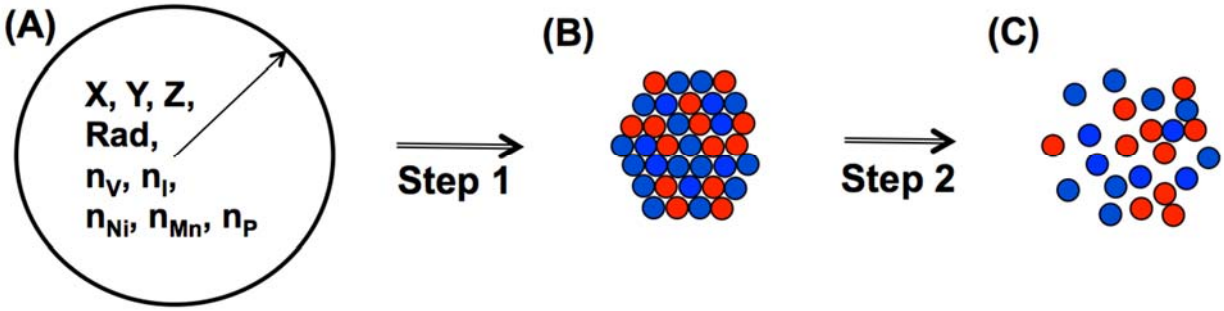

Fig. 3.5 – Two steps followed for mimicking the look by APT of our OKMC simulation box. (A) any defect in the simulation bow is described on an abstractive way, by its spatial coordinates (X,Y,Z), radius of interaction (Rad), and composition in term of vacancies (n_V), SIA (n_I), and solutes (n_{Ni}, n_{Mn}, n_P); (B) The solutes are virtually placed in the matrix, in the form of a compact cluster free of the Fe matrix, centred around the defect position; (C) Lattice distortions and loss of atoms are applied, in a realistic way compared to the APT.

The above-described procedure is relevant for performing a comparison of the predicted densities of solute-rich clusters. Comparing the sizes of these clusters is more delicate, however. Indeed, step 2 as illustrated in Fig. 3.5 can be regarded as a legitimate choice for a simplified model such as our OKMC, but it is most likely not representative of what happens in the real material. Solutes being constantly brought by individual carriers, we expect them to be actually deposited near SIA loops in a cloud fashion, as the carrying point defect supposedly detaches earlier from the solute due to elastic interactions with the loop. Additionally, SIA defects that are absorbed by the loop bring an additional content in Fe, diluting the solutes found around it. Finally, in real materials solute-rich clusters also have a content in Cr, which is not included in our present model. Regarding the large degree of uncertainty involved in these processes, estimating the actual radius of the resulting cloud of deposited solute atoms solely from physical considerations is delicate, and subjective to many arbitrary decisions. In view to perform a reasonable comparison with experimental data, we opted for an empirical approach. Given the solute content of the solute clusters as observed in APT, we computed the equivalent radii that those formed in our model would have, should they contain the same proportion of Fe and Cr atoms.

$$R = \left(\frac{3N}{8\pi S}\right)^{1/3} 1.5\, a_0 \qquad (2)$$

Here, N is the total number of solutes in the cluster, and S is the average minor solutes content in the APT measurements (Ni, Si and P only). The additional factor 1.5 takes into account the distortions of the atomic coordinates during the APT measurement, as discussed above.

The results obtained are summarized in Fig. 3.6. We see that, despite some arbitrary choices in the analysis, both the predicted density and size for the solute-rich clusters compare rather well with the experimental evidence. Clearly, the overall state of the microstructure at the final dose of the experiment, i.e. 0.6 dpa, are comparable, in spite of residual discrepancies in the densities, especially for the Fe-12%Cr alloy. A surprising observation, however, is that the model predicts a very early onset for the solute clusters. Indeed, already from 0.01 dpa, the density is as high as at 0.6dpa, but the average size is lower than 1.5 nm. Therefore, our expectation is that the observation by APT of these clusters, should they exist in the real material, would be particularly difficult. Only after 0.1 or even 0.2 dpa is the average size significantly increasing, which authorizes us to speculate that only from then on would the clusters become clearly visible in APT. Recent measurements (B. Gomez-Ferrer et al., University of Rouen, France) seem to confirm this scenario. APT investigation has been performed on Fe-9Cr and Fe12Cr neutron irradiated alloys at a dose of 0.06 dpa (MatISSE deliverable D2.3.1). Similar number density and sizes of solute clusters were found in both alloys namely: $(1.7 \pm 1.0)\ 10^{23}$ m^{-3} and $(1.2 \pm 0.7)\ 10^{23}$ m^{-3} for Fe-9Cr and Fe12Cr respectively and (1.3□ 0.6) nm and (1.4 □ 0.1) nm for Fe-9Cr and Fe12Cr. As predicted by the calculations, these figures are very close to those measured at 0.6 dpa.

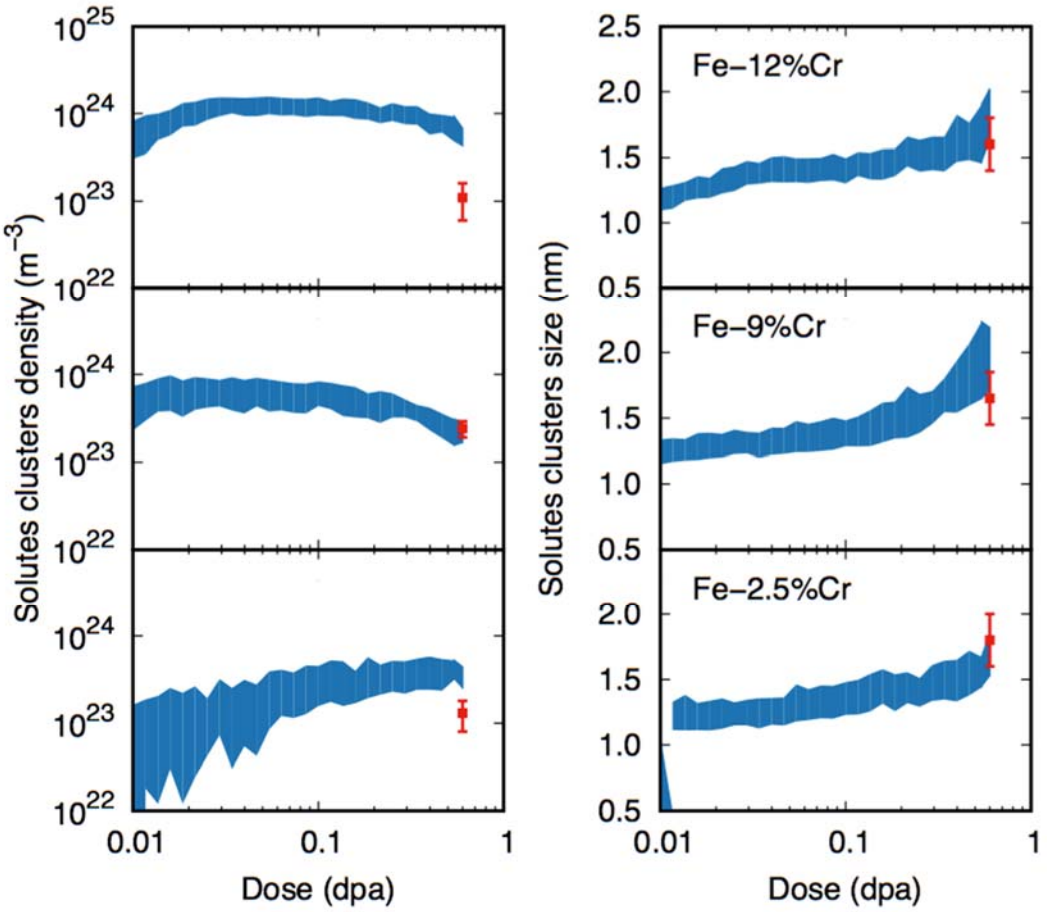

Fig. 3.6 – Evolution with the accumulated dose of the predicted population of APT-visible NiSiP-rich clusters, performed by our OKMC model (blue lines). Red dots are experimental data from Ref. [3,27,28]. The thickness of the blue line indicates the uncertainty of the processed data, assuming a threshold the minimal visible cluster size between 5 to 20 atoms.

Another instructive comparison between our model predictions and the experimental measurement with APT concerns the chemical composition of the solute clusters. Once again, an intermediate processing step is required. Since our model does not include Cr as solute atom, its content must be removed from the APT data. The Fe content must also be removed, for the same reasons as discussed in the previous paragraph. The comparison is shown in Fig. 3.7. We see that the chemical compositions differ for the Fe-2.5%Cr alloy, but they are rather similar for both the Fe-9%Cr and the Fe-12%Cr alloys.

Nonetheless, in these cases discrepancies with experimental data remain, which can be the consequence of several factors:

- The transport of solutes by single defects, parameterized assuming the infinite dilute limit, is debatable. In reality, multiple interactions in the matrix might break pairs earlier than otherwise predicted by DFT, thus favouring some solutes against the others.
- Solute clusters dissolution by crossing single point defects might be affected by the actual composition. In the present model, a single vacancy or a single SIA crossing a cluster grabs one solute at random, and carries it out. A more realistic parameterization, e.g., based on DFT-calculated binding energies, might favour the dissolution of some solutes against the others, depending on the composition.

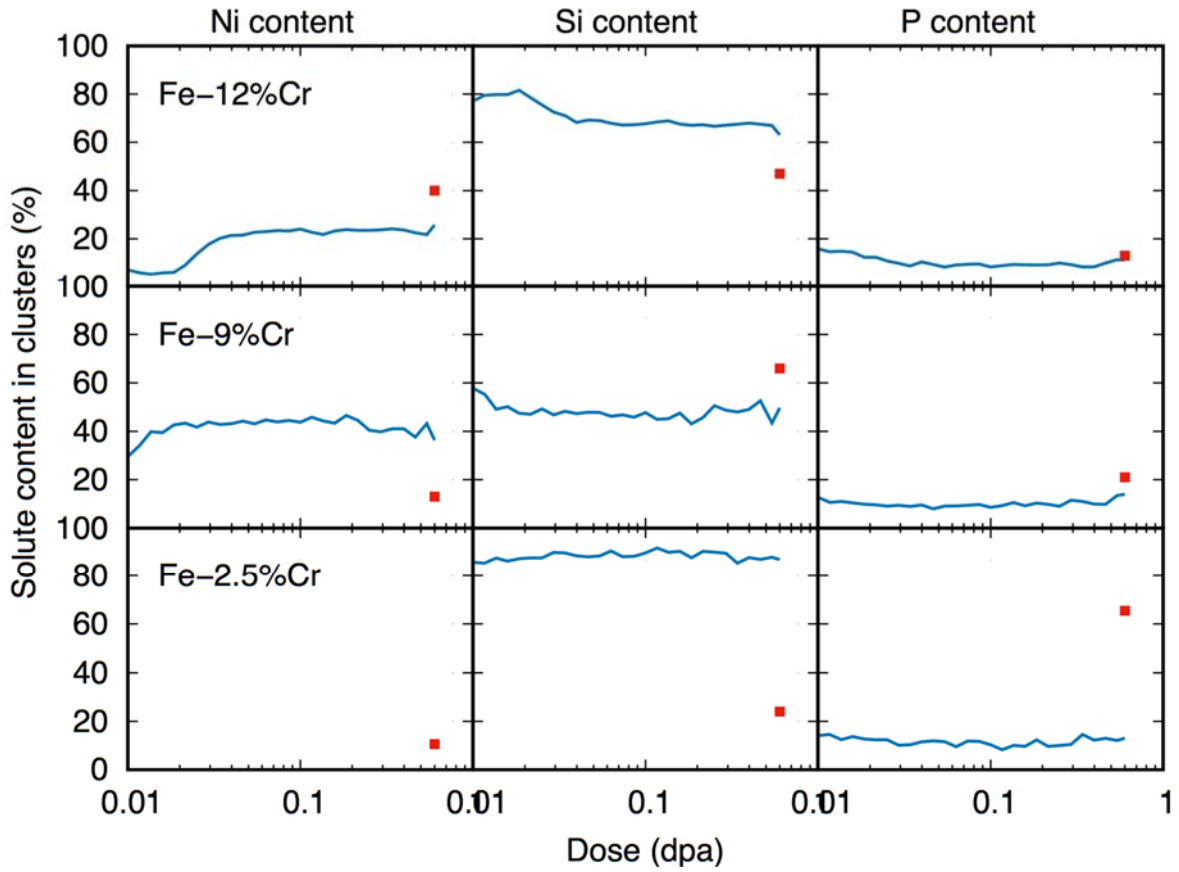

Fig. 3.7 – Comparison of the solute chemical composition as predicted by our OKMC model, with those measured experimentally by APT [3, 27,28]. In this later case, the data was here recalculated, ignoring both the Fe and Cr content.

3.3 Cellular model for the inclusion of Cr

The OKMC model reported in the previous sections do not include solute atoms explicitly. It is thus not suitable for predicting the formation of □' phases, nor to predict the Cr content in solute-rich clusters. Including Cr atoms in a similar way as the minor alloying elements in section 3.2 is not practically feasible, however. On the one hand, being in concentrated composition, simplifying assumptions such as those made for Ni, Si and P solutes would no longer be valid. At least, the transport of Cr atoms should ideally be described by adequate atomistic reactions, e.g., using an AKMC model thus taking the exact local atomic environment, while computing point defect migration energies. On the other hand, such detailed atomic descriptions are undesirable, because of the large computing time they require. For these reasons, a major upgrade of the model is required, using a dedicated level of abstraction for including the influence of the Cr content on the OKMC parameterisation. This was already partially performed in section 3.1 and section 3.2, as the grey alloy model accomplishes the same goal, assuming a constant and homogenous Cr content. Future improvement of the model should thus allow for a local component of the Cr content, without involving detailed atomic-level events.

Taking significant first steps towards this ambitious objective, we opted for the development of a cellular OKMC concept. In the following of this section, we report the work performed to demonstrate the feasibility of the concept. Preparing for a future modelling of full irradiation damage, we here consider single vacancies and single SIA's in binary FeCr alloys, without other solute elements.

3.3.1 Methodology

The model consists of dividing the computational box into smaller boxes (cells). In this model the actual positions of the alloying elements is not kept explicitly, but only the concentration on each one of the cells is known. For every defect in the simulation box, the probability of jumping to any of the neighboring sites is evaluated according to the local concentration and that of neighboring cells, biasing the migration with the difference in Gibbs free energy before and after the jump. The calculated rates are added to the usual kinetic Monte Carlo algorithm to select the particle appropriately. Once the particle jumps, the concentration of the alloy on each cell is updated accordingly depending on the type of defect that jumped.

The algorithm is explained here in more detail for the particular case of vacancies. A similar derivation can be done for self-interstitials.

Let's consider two cells, 1 & 2, with different alloy concentration and a single vacancy located in cell 1 (Fig.3.8). The two types of atoms in the system are A and B.

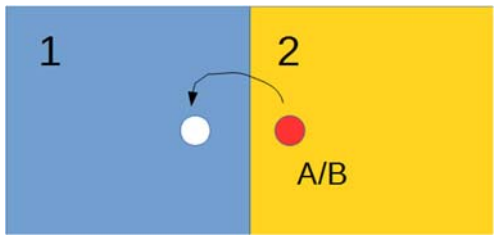

Fig. 3.8 – Diagram of two cells in the Cell-OKMC simulation box with different alloy concentration and one vacancy located in cell one, while an atom of type A or B jumps to that vacant site.

The total number of atoms in a perfect cell (without defects) is n. The total number of atoms in cell 1 is $n_1 = n_{A1} + n_{B1}$ where n_{A1} is the number of atoms of type A on cell 1 and n_{B1} is the total number of atoms of type B in cell 1. The number of atoms in cell 2 is: $n_2 = n_{A2} + n_{B2}$. In the example above, $n_1 = n - 1$ (since there is one vacancy) and $n_2 = n$.

The Gibbs free energy of this system is:

$$G_{TOT} = G_1 + G_2 \tag{3.3.1}$$

What we need to calculate is the difference in the free energy after the jump with respect to this initial energy:

$$\Delta G = G'_{TOT} - G_{TOT} = (G'_1 + G'_2) - (G_1 + G_2) \tag{3.3.2}$$

And we will bias the migration energy of the defect as:

$$E_m = E_{m0} + \frac{\Delta G}{2} \tag{3.3.3}$$

where E_{m0} is the migration energy of the defect in the cell. It is important to point out that in our first implementation, we considered this as the migration energy of the defect in the pure metal (independent of concentration). In the latest implementation of the method, the migration energy depends on the local concentration.

The Gibbs free energy of each cell can be calculated as:

$$G_1 = n_{A1}\mu_A^0 + n_{B1}\mu_B^0 + n_1 \Delta G_{mix}(C_1) \quad (3.3.4a)$$

$$G_2 = n_{A2}\mu_A^0 + n_{B2}\mu_B^0 + n_2 \Delta G_{mix}(C_2) \quad (3.3.4b)$$

$$G'_1 = n'_{A1}\mu_A^0 + n'_{B1}\mu_B^0 + n'_1 \Delta G_{mix}(C'_1) \quad (3.3.4c)$$

$$G'_2 = n'_{A2}\mu_A^0 + n'_{B2}\mu_B^0 + n'_2 \Delta G_{mix}(C'_2) \quad (3.3.4d)$$

where $\mu^0_{A/B}$ is the chemical potential of atoms A/B, $C_{1(2)}$, $C'_{1(2)}$ are the concentrations in cells 1 (or 2) before and after the jump respectively, and ΔG_{mix} is the mixing enthalpy of Levesque et al. [19].

Let's consider the case where an atom of type B jumps from cell 2 to cell 1. The number of atoms after this jump on each cell is:

$$n'_{A1} = n_{A1} \quad (3.3.5a)$$

$$n'_{B1} = n_{B1} + 1 \quad (3.3.5b)$$

$$n'_{A2} = n_{A2} \quad (3.3.5c)$$

$$n'_{B2} = n_{B2} - 1 \quad (3.3.5d)$$

$$n'_1 = n_1 + 1 \quad (3.3.5e)$$

$$n'_2 = n_2 - 1 \quad (3.3.5f)$$

Considering all the above equations we can calculate the change in energy and we get to the expression:

$$\Delta G = (n_1+1)\Delta G_{mix}(C'_1) - n_1 \Delta G_{mix}(C_1) + (n_2 - 1)\Delta G_{mix}(C'_2) - n_2 \Delta G_{mix}(C_2) \quad (3.3.6)$$

If we consider that an atom of type A that jumps from cell 2 to cell 1, we arrive to exactly the same expression, but the final concentrations, C'_1, C'_2 are different depending on whether the atom that jumps is type A or type B.

If an atom of type B jumps:

$$C'_1 = \frac{n_{B1}+1}{n_{B1}+n_{A1}+1} \quad (3.3.7a)$$

$$C'_2 = \frac{n_{B2}-1}{n_{B2}+n_{A2}-1} \quad (3.3.7b)$$

If an atom of type A jumps:

$$C'_1 = \frac{n_{B1}}{n_{B1}+n_{A1}+1} \quad (3.3.7c)$$

$$C'_2 = \frac{n_{B2}}{n_{B2}+n_{A2}-1} \quad (3.3.7d)$$

The initial concentrations are:

$$C_1 = \frac{n_{B1}}{n_{B1}+n_{A1}} \quad (3.3.7e)$$

$$C'_2 = \frac{n_{B2}}{n_{B2}+n_{A2}} \quad (3.3.7f)$$

If we do the approximation that the change in concentration is very small compared to the actual concentration, we can arrive to a different expression for the change in total energy.

$$C' = C + \Delta C \quad \text{If } \Delta C \ll C$$

$$\Delta G_{mix}(C') \;\; \Delta G_{mix}(C)+\frac{dG_{mix}}{C}\Delta C=\Delta G_{mix}(C)+\mu\Delta C \tag{3.3.8}$$

Using this approximation we arrive at the following expression for the change in energy:

$$\Delta G=(n_1+1)\frac{d\Delta G_{mix}(C_1)}{dC}\Delta C_1+(n_2-1)\frac{d\Delta G_{mix}(C_2)}{dC}\Delta C_2+(\Delta G_{mix}(C_1)-\Delta G_{mix}(C_2)) \tag{3.3.9}$$

where $d\Delta G_{mix}/dC$ is the derivative of the change of free energy with respect to the concentration.

Here we can make some calculations to remove the explicit dependency on the number of lattice atoms n_1 and n_2. Assuming an exchange of Cr between cell#1 and cell#2:

$Cr_{2\rightarrow1}$

$$C_1=\frac{n_{Cr1}}{n_1}\quad C'_1=\frac{n_{Cr1}+1}{n_1+1}=\frac{C_1n_1+1}{n_1+1}\quad \Delta C_1=C'_1-C_1=\frac{C_1n_1+1}{n_1+1}-C_1=\frac{C_1n_1+1-C_1n_1-C_1}{n_1+1}=\frac{1-C_1}{n_1+1}$$

$$C_2=\frac{n_{Cr2}}{n_2}\quad C'_2=\frac{n_{Cr2}-1}{n_2-1}=\frac{C_2n_2-1}{n_2-1}\quad \Delta C_2=C'_2-C_2=\frac{C_2n_2-1}{n_2-1}-C_2=\frac{C_2n_2-1-C_2n_2+C_2}{n_2-1}=\frac{C_2-1}{n_2-1}$$

applying these two equations for the variation in concentration in both cells to the equation of the variation of the free energy we get

$$\Delta G=\frac{d\Delta G_{mix}(C_1)}{dC}(1-C_1)+\frac{d\Delta G_{mix}(C_2)}{dC}(C_2-1)+(\Delta G_{mix}(C_1)-\Delta G_{mix}(C_2))$$

and now, assuming an exchange of Fe between the cells:

$Fe_{2\rightarrow1}$

$$C_1=\frac{n_{Cr1}}{n_1}\quad C'_1=\frac{n_{Cr1}}{n_1+1}=\frac{C_1n_1}{n_1+1}\quad \Delta C_1=C'_1-C_1=\frac{C_1n_1}{n_1+1}-C_1=\frac{C_1n_1-C_1n_1-C_1}{n_1+1}=\frac{-C_1}{n_1+1}$$

$$C_2=\frac{n_{Cr2}}{n_2}\quad C'_2=\frac{n_{Cr2}}{n_2-1}=\frac{C_2n_2}{n_2-1}\quad \Delta C_2=C'_2-C_2=\frac{C_2n_2}{n_2-1}-C_2=\frac{C_2n_2-C_2n_2+C_2}{n_2-1}=\frac{C_2}{n_2-1}$$

analogously to the previous case, we get the following expression for the variation of the free energy

$$\Delta G=\frac{d\Delta G_{mix}(C_1)}{dC}(-C_1)+\frac{d\Delta G_{mix}(C_2)}{dC}(C_2)+(\Delta G_{mix}(C_1)-\Delta G_{mix}(C_2))$$

Both approximations have been implemented in the OKMC code MMonCa, giving practically the same results. Besides these two implementations, another expression was derived by G. Bonny. The above seems to be the one that gives the best result so far, although further analysis of the method developed by G. Bonny should be done.

This approach has been tested by calculating the phase diagram of Fe-Cr. Our initial implementation gave rise to a difference at high Cr concentrations of the results obtained from the method and those calculated from the Levesque expression [19], the OKMC results gave lower Cr concentrations than the expected values. A significant effort was put into solving this discrepancy. A thorough analysis showed that two factors influence

this result. On one hand using a migration energy (E_{m0}) that depends on the local concentration, but mostly the way the type of neighbouring sites is selected. In our first implementation only 6 sites were considered as neighbours for each atom, assuming that defects jump to the six faces of a cube. This has now been changed to jumps to 8 neighbours, therefore considering the b.c.c. structure. Since we do not have explicitly the location of the Cr atoms, the type of neighbour is selected according to the Cr concentration of that cell. We have noticed that the selection of the type of atom also plays a role in reaching the equilibrium concentration expected from the phase diagram. With the above mentioned improvements to the model we have been able to obtain a phase-diagram that is quite close to the one expected from the Levesque expression, as shown in Fig. 3.9.

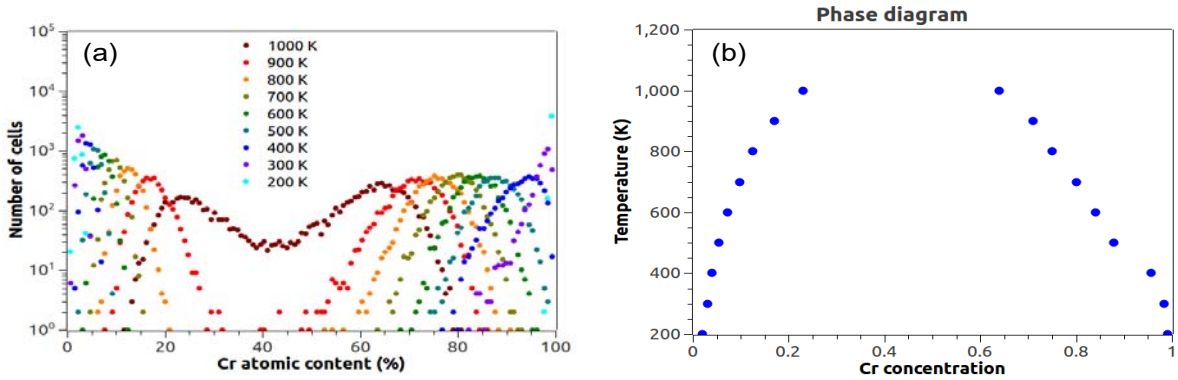

Fig. 3.9 – Calculation of the phase-diagram of FeCr (a) profile of concentrations of different cells in the simulation box for different temperatures (b) Phase-diagram obtained from the maximum of the peaks at each temperature in (a).

These calculations are performed considering an initial concentration of 50% Cr and one single vacancy in the whole Cell-OKMC simulation box. The system is allowed to evolve at different temperatures, giving rise to the separation in two phases, a low and a high concentration phase, as shown in the profiles of Fig. 3.9(a). Here the concentration on each of the cells in the Cell-OKMC is represented, and for temperatures below 1000K, two distinct peaks are obtained. From the maximum of these peaks we can construct the phase diagram shown in Fig. 3.9(b). Here, at high Cr concentrations and low temperatures, the Cr concentration is close to 1, as expected from the Levesque's expression.

Fig. 3.10 shows three snapshots of the simulation cell for three different temperatures, 300K, 600K and 900K where the phase separation is clear for the lowest temperatures and more diffuse for the highest one, as expected.

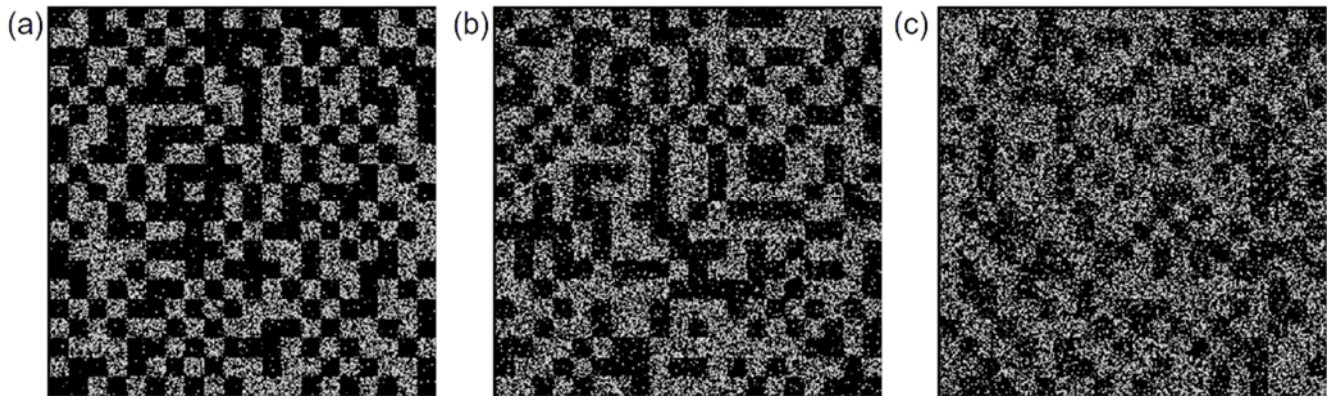

Fig. 3.10 – Snapshots of the Cell-OKMC simulation cell for (a) 300K (b) 600K and (c) 900K where the phase separation can be observed.

3.3.2 Results

The model described above has been used to study segregation of Cr to a grain boundary due to the presence of point defects, vacancies and self-interstitials. The grain boundary is modelled in the simplest way: an internal surface that act as a perfect sink for all defects arriving to it within a certain capture radius. Defects are created with a dose rate of 1.2×10^{-5} dpa/s, which correspond to that used in the experiments by J. P. Wharry and G. S. Was [12] for proton irradiation of T91. In these calculations defects are allowed to cluster. However, binding energies of clusters or interaction radius of defects with clusters are considered as those for pure Fe, and used in previous calculations by our group [3].

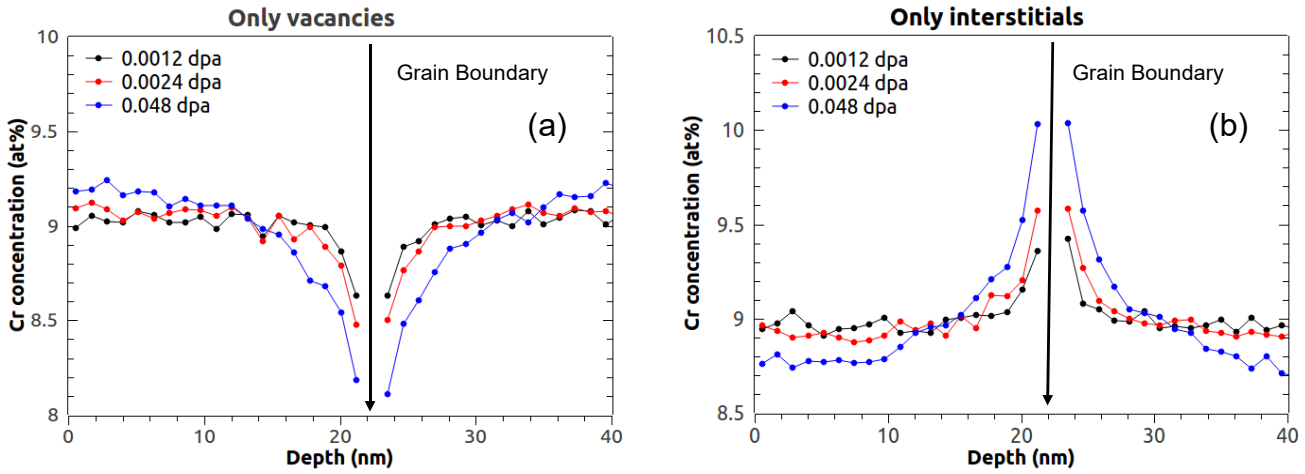

Fig. 3.11 – Segregation of Cr in the presence of point defects and a grain boundary (a) only vacancies (b) only self-interstitials at 300°C and different irradiation doses.

Fig 3.11 shows the concentration of Cr across the simulation box. The grain boundary is located in the centre of the box. We can see from these results that the method is providing the expected trend: when only vacancies are present Cr segregates away from the grain boundary giving rise to a depletion next to the grain boundary (Fig 3.11(a)), while in the presence of self-interstitials, Cr segregates towards the grain boundary (Fig 3.11(b)) showing an enrichment. These results are for a temperature of 300ºC and a Cr concentration of 9%, close to the values in [12].

Fig. 3.12 shows the temperature dependence for a fixed dose, 0.048 dpa and for the case of only vacancies or only self-interstitials in the simulation box.

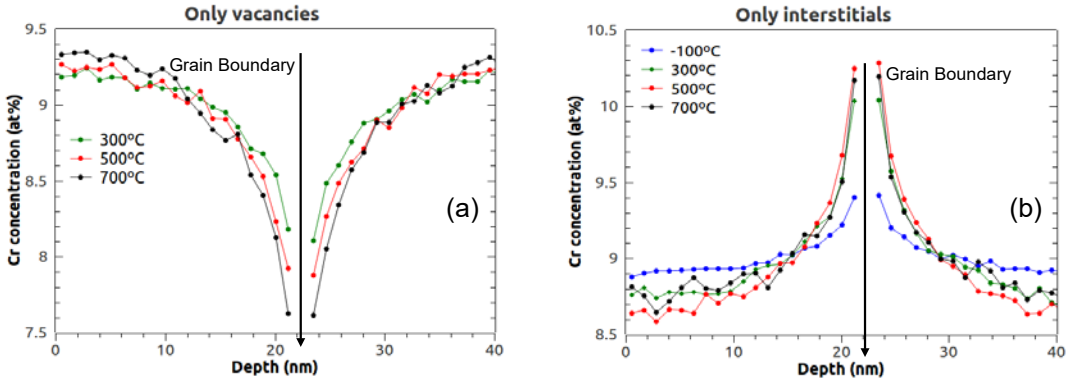

***Fig. 3.12** – Temperature dependence of Cr profiles for a fixed dose, 0.048 dpa for the case of (a) only vacancies and (b) only self-interstitials.*

No changes in Cr concentration are observed for low temperatures (below 300ºC) while in the case of self-interstitials we can observed the enrichment of the grain boundary even at very low temperature (-100ºC) due to their fast migration. The fast migration of self-interstials can also be observed from the fact that the profiles are very similar for all temperatures 300ºC and above.

When Frenkel-pairs are considered (vacancies and self-interstitials created at the same rate), we observed a slight enhancement at very low temperature. However, at 300ºC we do not see any differences in the Cr profile across the simulation cell, as shown in Fig. 3.13.

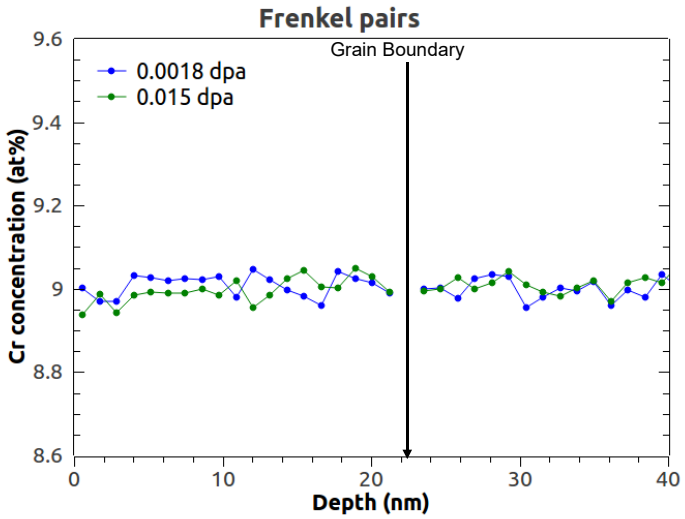

Fig. 3.13 – Concentration of Cr for two different doses in the presence of Frenkel-pairs at 300°C.

The reason for this result is that vacancies and self-interstitials are recombining both in the bulk and at the grain boundary, giving rise to a cancellation of the effects of each one of these defects.

3.3.3 Conclusions

The Cell-OKMC model has been improved to better reproduce the phase diagram of FeCr. Most of the improvements where related to values of the migration energy depending on local concentration and the way the neighboring atoms are selected. This improved model has been used to study segregation of Cr to grain boundaries. The model shows the correct behaviour: depletion at the grain boundary in the presence of vacancies and enrichment in the case of self-interstitials. However, when including Frenkel pairs since the same ammount of vacancies and self-interstitials arrives to the interface no changes are observed, except for very low temperatures, where vacancy migration is negligible.

Several changes must be implemented to model FeCr properly. Currently, all self-interstitials are considered to be mixed dumbbells and migrate as such through the whole simulation. However, the possibility of dissociation of this dumbbell and formation of pure Fe dumbbells should be included.

4 Discussions and future perspectives

In this work, we proposed a physically-based model for describing the mechanism leading to the formation of solute-rich clusters in F/M steels. Intrinsically assuming a radiation-induced driving force, solute atoms are described as being dragged by single point defects, until the latter are eliminated at sinks. We started by carefully porting an OKMC model initially developed for the FeC system, towards the Fe-C-Cr model alloy. A grey alloy approximation was then used for taking the Cr content into account. Next, consistently with our initial hypotheses, the refined OKMC model including minor solute elements, confirmed that the sinks for Vac-solutes and SIA-solutes pairs are for the most SIA loops, whose majority is invisible to the TEM because of their small size.

The results obtained in section 3 are very encouraging. They prove that our basic hypotheses for the mechanism leading to the formation of solute-rich clusters, responsible for hardening and embrittlement in F/M steels, is plausible. Starting by a microstructural model and then upgrading it with a simple treatment for the minor solutes, we approached the problem taking the simplest angle. Essentially, our model assumes the radiation-induced driving force entirely, disregarding the thermodynamics aspect. It is only parameterized by a couple of binding energies, letting thus room for improvement:

- Dragging of the solutes from the matrix towards sinks can be more realistically described. One possible approach is to calculate effective transport coefficients in random dilute matrices, using a relevant energy model. Fitting EAM-like interatomic potentials may be too hard for this purpose. An alternative approach could be either cluster expansion models [45], or neural-network-potentials [46], directly fitted on DFT.
- Binding energies between SIA loops and decorating solutes should also be more realistically parameterized. Once again, this could be addressed by a campaign of DFT calculations. To tackle the practical problem of integrating this information into the model, we envision that dedicated artificial neural networks can be designed for such purpose, similarly to our enhanced AKMC model [47] where they are used to predict accurate vacancy migration energies. Given as input a description of a loop (e.g. the number of SIA contained) and of the cloud of decorated solutes, these ANN would be trained to make a prediction for the effective binding energy.

The major next step for improving the model is to merge the OKMC tools proposed in section 3.2 and section 3.2. By integrating the cellular treatment of the Cr into the classical OKMC dealing with minor solutes, it would be possible to make complete predictions for all the nanofeatures observed experimentally, i.e., □', and CrNiSiP-rich clusters.

Finally, the models here presented are not dealing with heterogeneous precipitation. This aspect can be specifically addressed in the future, by including an explicit dislocation line in our simulation box.

5 References

[1] M. Hernandez-Mayoral et al., Deliverable D4.9, GETMAT FP7-Project, (2013).
[2] M. Hernandez-Mayoral et al., J. Nucl. Mater. 474 (2016) 88.
[3] V. Kuksenko et al., J. Nucl. Mater. 415 (2011) 61; V. Kuksenko et al., J. Nucl. Mater. 432 (2013) 160.
[4] C. Heintze et al., J. Physics: Conf. Series 247 (2010) 012035.
[5] C. Pareige et al., J. Nucl. Mater. 456 (2015) 471.
[6] F. Bergner et al., J. Nucl. Mater. 448 (2014) 96.
[7] Matisse Deliverable D2.2.2.
[8] M. Bachhav et al., J. Nucl. Mater. 453 (2014) 334.
[9] M. Bachhav et al. J. Nucl. Mater. 454 (2014) 381.
[10] G. Bonny et al. J. Nucl. Mater. 452 (2014) 486.
[11] D. Terentyev et al. Scripta Mater. 62 (2010) 697.
[12] D. Terentyev et al. Acta Mater. 61 (2013) 1444; D. Terentyev et al. J. Nucl. Mater. 442 (2013) 470.
[13] O. Senninger, F. Soisson, E. Martínez, M. Nastar, C.-C. Fu, Y. Bréchet, Acta Mater. 103 (2016) 1–11.
[14] F. Soisson, T. Jourdan, Acta Mater. 103 (2016) 870–881.
[15] F. Soisson, E. Meslin, O. Tissot, submitted to Acta Mater.
[16] M. Bachhav, G. Robert Odette, E.A. Marquis, Scr. Mater. 74 (2014) 48–51.
[17] H. Saitoh, N. Yoshinaga, K. Ushioda, Acta Mater. 52 (2004) 1255–1261.
[18] I.S. Golovin, M.S. Blanter, R. Schaller, Phys. Status Solidi A 160 (1997) 49–60.
[19] M. Levesque, et al. Phys. Rev. B 84, 184205 (2011)
[20] J. P. Wharry, G. S. Was, J. Nucl. Mat. 442 (2013) 7
[21] V. Jansson et al., J. Nucl. Mat. 442 (2013) 341.
[22] M. Chiapetto et al., J. Nucl. Mat. 465 (2015) 326.
[23] M. Chiapetto et al., Nuc. Mat. Ener. 9 (2016) 565.
[24] M. Hernandez-Mayoral et al., J. Nucl. Mater. (2014).

[25] M. Matijasevic, A. Almazouzi, J. Nucl. Mater. 377 (2008) 147.
[26] D. Terentyev, P. Olsson, L. Malerba, A.V. Barashev, J. Nucl. Mater. 362 (2007) 167.
[27] E. Meslin et al., J. Nucl. Mater. 399 (2010) 137.
[28] E. Meslin et al., J. Nucl. Mater. 406 (2010) 73.
[29] N. Castin et al., J. Nucl. Mater. 429 (2012) 315.
[30] K. Arakawa, M. Hatanaka, H. Mori, K. Ono, J. Nucl. Mater. 329-333 (2004) 1194.
[31] M. Hernandez-Mayoral, Z. Yao, M.L. Jenkins, M.A. Kirk, Philos. Mag. 88 (2008) 2881.
[32] Z. Yao, M. Herna ndez-Mayoral, M.L. Jenkins, M.A. Kirk, Philos. Mag. 88 (2008) 2851.
[33] M.L. Jenkins, Z. Yao, M. Herna ndez-Mayoral, M.A. Kirk, J. Nucl. Mater. 389 (2009) 197.
[34] D. Terentyev, P. Olsson, L. Malerba, J. Nucl. Mater. 386e388 (2009) 140e142.
[35] D. Terentyev, L. Malerba, A.V. Barashev, Philos. Mag. Lett. 85 (2005) 587e594.
[36] D. Terentyev, P. Olsson, L. Malerba, A.V. Barashev, J. Nucl. Mater. 362 (2007) 167e173.
[37] D. Terentyev, L. Malerba, A. Barashev, Philos. Mag. 88 (2008) 21.
[38] D. Terentyev, M. Klimenkov, L. Malerba, J. Nucl. Mater. 393 (2009) 30e35.
[39] N. Anento, A. Serra, J. Nucl. Mater. 440 (2013) 236.
[40] D. Terentyev, N. Anento, A. Serra, V. Jansson, H. Khater, G. Bonny, J. Nucl. Mater. 408 (2011) 272.
[41] L. Messina, M. Nastar, T. Garnier, C. Domain and P. Olsson, Phys. Rev. B 90 (2014) 104203
[42] L. Messina et al., submitted to Phys. Rev. B.
[43] C. Pareige, P. Pareige, B. Radiguet, and G. DaCosta, Private communication in the framework of the FP7/NUGENIA-PLUS APLUS project.
[44] J. Hyde, G. DaCosta, C. Hatzoglou, H. Weekes, B. Radiguet, P. Styman, F. Vurpillot, C. Pareige, A. Etienne, G. Bonny, N. Castin, L. Malerba, and P. Pareige, Microsc. Microanal. 23, 366 (2017).
[45] G. Bonny et al., submitted for publication.
[46] N. Castin, L. Messina, C. Domain, R.C. Pasianot and P. Olsson, Phys. Rev. B 95 (2017) 214117.
[47] N. Castin and L. Malerba, J. Chem. Phys. 132 (2010) 074507.